

**REPORT DOCUMENTATION PAGE**

Form Approved OMB No. 0704-0188

Public reporting burden for this collection of information is estimated to average 1 hour per response, including the time for reviewing instructions, searching existing data sources, gathering and maintaining the data needed, and completing and reviewing the collection of information. Send comments regarding this burden estimate or any other aspect of this collection of information, including suggestions for reducing the burden, to Department of Defense, Washington Headquarters Services, Directorate for Information Operations and Reports (0704-0188), 1215 Jefferson Davis Highway, Suite 1204, Arlington, VA 22202-4302. Respondents should be aware that notwithstanding any other provision of law, no person shall be subject to any penalty for failing to comply with a collection of information if it does not display a currently valid OMB control number.

**PLEASE DO NOT RETURN YOUR FORM TO THE ABOVE ADDRESS.**

<b>1. REPORT DATE (DD-MM-YYYY)</b> 01-09-2008	<b>2. REPORT TYPE</b> Final Report	<b>3. DATES COVERED (From – To)</b> 25 September 2006 – 25 March 2008
--	---------------------------------------	--

<b>4. TITLE AND SUBTITLE</b>  Measurements of Two-Cell Flux Qubits at Millikelvin Temperatures	<b>5a. CONTRACT NUMBER</b> FA8655-06-1-3090
	<b>5b. GRANT NUMBER</b> Grant 06-3090
	<b>5c. PROGRAM ELEMENT NUMBER</b> 61102F

<b>6. AUTHOR(S)</b>  Professor Alexey Ustinov	<b>5d. PROJECT NUMBER</b>
	<b>5d. TASK NUMBER</b>
	<b>5e. WORK UNIT NUMBER</b>

<b>7. PERFORMING ORGANIZATION NAME(S) AND ADDRESS(ES)</b> Physikalisches Institut III Karlsruhe D-76131 Germany	<b>8. PERFORMING ORGANIZATION REPORT NUMBER</b>  N/A
--	--

<b>9. SPONSORING/MONITORING AGENCY NAME(S) AND ADDRESS(ES)</b>  EOARD Unit 4515 BOX 14 APO AE 09421	<b>10. SPONSOR/MONITOR'S ACRONYM(S)</b>
	<b>11. SPONSOR/MONITOR'S REPORT NUMBER(S)</b> Grant 06-3090

**12. DISTRIBUTION/AVAILABILITY STATEMENT**  
Approved for public release; distribution is unlimited.

**13. SUPPLEMENTARY NOTES**

**14. ABSTRACT**

We report on the study of Josephson junction two-cell flux qubits and phase qubits. We have made progress with fabrication of two-cell flux qubits based on small Al-AIOx-Al Josephson tunnel junctions. We succeeded in preparing junctions as small as 0.09 to 0.24 micrometers squared. We describe newly developed sample design which implements a "silent" two cell qubit containing a fluxon trapping loop as a phase shifter. This design was submitted for fabrication at MIT Lincoln Lab foundry. We characterized several chips fabricated according to this design at MIT Lincoln Laboratory and observed a switching of the qubit from one classical state to the other. A new readout scheme which uses fast current pulses is under development. The states of superconducting quantum bits, as the Josephson ux and phase qubits, are distinguished by magnetic ux generated by a persistent current in a superconducting loop. This ux is read out by measuring the switching current of an inductively coupled SQUID detector. As the readout circuit contributes decoherence, its coupling to the qubit should be made as weak as possible. In the second part of this report, we demonstrate a new data evaluation method which maximizes the measurement contrast of the two qubit states, thus allowing to significantly decrease the coupling. The method is tested experimentally by measuring high-fidelity Rabi oscillations in phase qubits operated beyond the single-shot resolution limit. This technique is promising for multi-qubit circuits since it allows to read out the states of several qubits by a single weakly coupled SQUID. Our current work on Josephson phase qubits is focussed on the study of temperature effects on decoherence. Using samples fabricated from different materials and origins, we measured Rabi and Ramsey oscillations in a wide range of temperatures. Unexpectedly, the decoherence times extracted from the data show only a very weak dependence on temperature. We find that coherent operation of the qubits remains possible as long as the thermal energy kB T is smaller than the energy difference between the qubit eigenstates. Since the latter is determined by the circuit design, it makes possible operating currently available superconducting qubits at temperatures of 300 mK and even higher.

--

**15. SUBJECT TERMS**

EOARD, Quantum Bits, Physics, Information Technology, Quantum Information Processing

<b>16. SECURITY CLASSIFICATION OF:</b>			<b>17. LIMITATION OF ABSTRACT</b> SAR	<b>18, NUMBER OF PAGES</b>  25	<b>19a. NAME OF RESPONSIBLE PERSON</b> SCOTT DUDLEY, Lt Col, USAF
<b>a. REPORT</b> UNCLAS	<b>b. ABSTRACT</b> UNCLAS	<b>c. THIS PAGE</b> UNCLAS			<b>19b. TELEPHONE NUMBER</b> <i>(Include area code)</i> +44 (0)1895 616162

**Standard Form 298** (Rev. 8/98)  
Prescribed by ANSI Std. Z39-18

Final Report (No. 4)

# Measurements of Two-Cell Flux Qubits at Millikelvin Temperatures

A. K. Feofanov, J. Lisenfeld and A. V. Ustinov

Physikalisches Institut III, Universität Erlangen-Nürnberg  
D-91058 Erlangen, Germany

Supported by European Office of Aerospace Research and Development (EOARD)  
under Contract FA8655-06-1-3090

September 2008

# Contents

<b>Abstract</b>	<b>2</b>
<b>1 Two-cell flux qubits</b>	<b>2</b>
1.1 “Silent” two-cell qubit . . . . .	2
1.2 Nb/AlO <sub>x</sub> /Nb junction based qubits . . . . .	3
1.2.1 Samples fabricated at MIT Lincoln Laboratory . . . . .	3
1.2.2 Measurements . . . . .	5
1.2.3 New design submitted to MIT Lincoln Lab . . . . .	7
1.3 Al/AlO <sub>x</sub> /Al junction based qubits . . . . .	7
1.3.1 Fabrication in Erlangen . . . . .	7
1.3.2 Measurements . . . . .	9
<b>2 High-contrast readout of superconducting qubits</b>	<b>12</b>
2.1 Motivation . . . . .	12
2.2 The Josephson phase qubit . . . . .	12
2.3 Switching-current readout using a dc-SQUID . . . . .	13
2.4 Data evaluation procedure . . . . .	13
2.5 Experimental results . . . . .	14
2.6 Application in multi-qubit circuits . . . . .	14
<b>3 Josephson phase qubits</b>	<b>15</b>
3.1 Samples . . . . .	16
3.2 Spectroscopic quality factor . . . . .	17
3.3 Coherent oscillation at high temperatures . . . . .	18
<b>4 Summary and conclusion</b>	<b>18</b>
<b>References</b>	<b>22</b>

## Abstract

We report on the study of Josephson junction two-cell flux qubits and phase qubits. We have made progress with fabrication of two-cell flux qubits based on small Al-AlO<sub>x</sub>-Al Josephson tunnel junctions. We succeeded in preparing junctions as small as  $0.09 \times 0.24 \mu\text{m}^2$ . We describe newly developed sample design which implements a “silent” two-cell qubit containing a fluxon trapping loop as a phase shifter. This design was submitted for fabrication at MIT Lincoln Lab foundry. We characterized several chips fabricated according to this design at MIT Lincoln Laboratory and observed a switching of the qubit from one classical state to the other. A new readout scheme which uses fast current pulses is under development.

The states of superconducting quantum bits, as the Josephson flux and phase qubits, are distinguished by magnetic flux generated by a persistent current in a superconducting loop. This flux is read out by measuring the switching current of an inductively coupled SQUID detector. As the readout circuit contributes decoherence, its coupling to the qubit should be made as weak as possible. In the second part of this report, we demonstrate a new data evaluation method which maximizes the measurement contrast of the two qubit states, thus allowing to significantly decrease the coupling. The method is tested experimentally by measuring high-fidelity Rabi oscillations in phase qubits operated beyond the single-shot resolution limit. This technique is promising for multi-qubit circuits since it allows to read out the states of several qubits by a single weakly coupled SQUID.

Our current work on Josephson phase qubits is focussed on the study of temperature effects on decoherence. Using samples fabricated from different materials and origins, we measured Rabi and Ramsey oscillations in a wide range of temperatures. Unexpectedly, the decoherence times extracted from the data show only a very weak dependence on temperature. We find that coherent operation of the qubits remains possible as long as the thermal energy  $k_B T$  is smaller than the energy difference between the qubit eigenstates. Since the latter is determined by the circuit design, it makes possible operating currently available superconducting qubits at temperatures of 300 mK and even higher.

## 1 Two-cell flux qubits

The flux qubits use junctions enclosed in superconducting loops as quantum coherent systems. *Single-cell* flux qubits have been previously studied at MIT and Delft. These devices have already shown quantum superposition of macroscopic persistent current states and quantum-coherent oscillations in direct time-resolved measurements. We are focusing on *two-cell* flux qubits consisting of four identical Josephson tunnel junctions. These devices have an advantage of having a control over the barrier height between two potential wells.

### 1.1 “Silent” two-cell qubit

We developed a new scheme for two-cell flux qubits which we call a “silent” qubit. Its main idea can be seen from Fig. 1. Having a flux quantum trapped permanently in the inner loop, the qubit has the advantage of using smaller range of magnetic fields for the symmetric flux control. The trapped flux serves as  $\pi$ -shifter of the phase and contributes equally to the phase change in both loops. Thus one does not need to apply large external flux and the qubit is operated close to zero symmetric field. In order to avoid steep dependence of qubit level splitting on magnetic field, we can make junctions in outer qubit loop smaller as suggested recently by Dr. Stanford Yukon.

A two cell flux qubit contains four Josephson junctions of two different sizes. Two outer Josephson junctions numbered #3 and #4 have smaller area than two inner ones numbered #1 and #2. We denote by  $\rho$  the ratio between their critical currents and thus their Josephson

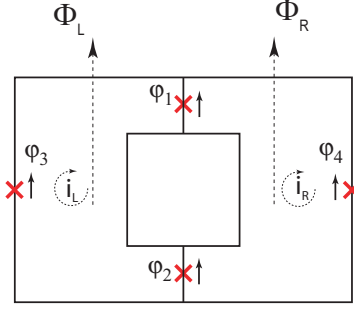


Figure 1: A “silent” two-cell flux qubit

energies:

$$E_J^{(3,4)} = \rho E_J^{(1,2)}, \quad (1)$$

The potential energy  $U$  of the qubit is periodic as a function of the average phase  $\chi = 0.5(\varphi_1 + \varphi_2)$  on junctions #1 and #2:

$$U = -2 \cos \chi + r \cos(2\chi - \phi_a). \quad (2)$$

Here  $r = -2\rho \cos(\phi_s)$ , while  $\phi_s = \frac{\phi_L + \phi_R}{2}$  and  $\phi_a = \frac{\phi_L - \phi_R}{2}$  are the symmetric and anti-symmetric parts of the flux in the two cells, respectively. Each period of  $U(\chi)$  has two minima. For  $\rho = r/2$  we can operate this qubit at half frustration in each cell. With a single flux quantum  $\Phi_0$  frozen in the inner loop this would require zero or (in non-ideal case) a very small external magnetic field. The inner loop thus acts as passive  $\pi$ -shifter. The potential (2) has two minima associated with the circulating currents in the outer loops, as shown in Fig. 2. At the optimal working point of  $r = 0.76$ , the current through the central line changes from state (a) to state (b) by approximately  $2I_c^{(3,4)} = 2\rho I_c^{(1,2)}$ .

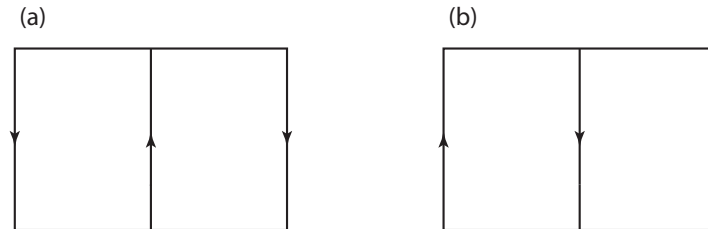


Figure 2: Two states of the two-cell flux qubit shown in Fig. 1. The arrows show the flow directions of the persistent currents.

In quantum regime, at the optimal operating point the mean current through every Josephson junction is zero. Taking into account that we work near zero external magnetic field, it means that at the operating point the “silent” qubit is practically decoupled from the fluctuations caused by the flux control and readout lines.

## 1.2 Nb/AIO<sub>x</sub>/Nb junction based qubits

### 1.2.1 Samples fabricated at MIT Lincoln Laboratory

At the end of December 2006 we submitted a new design to MIT Lincoln Laboratory foundry. We designed a readout circuit to measure the “silent” qubit described above. This circuit contains an asymmetric three-junction dc-SQUID inductively coupled to the qubit. The SQUID has sufficient flux sensitivity at zero external magnetic field. The qubit is placed

inside the readout SQUID loop, which is coupled asymmetrically to the two cells of the qubit. The flux through the SQUID loop changes when the qubit switches between two persistent current states. The targeted critical current  $I_{Cq}$  of inner qubit junctions is about  $0.5 \mu\text{A}$  and capacitance  $C_q \approx 5.8 \text{ fF}$ . The outer qubit junctions are designed 2.5 times smaller than the inner ones. The calculated level splitting of the qubit is around  $\omega_{01} \approx 1.5 \text{ GHz}$  at the working point  $r = 0.8$ . We optimized self and mutual inductances of the qubit cells and the readout SQUID to have the change of the flux through the SQUID loop induced by qubit switching between two states to be about  $\Delta\Phi \approx 0.002 \Phi_0$ . Sizes of junctions were optimized for three announced critical current densities of  $500 \text{ A/cm}^2$ ,  $1 \text{ kA/cm}^2$  and  $2 \text{ kA/cm}^2$ . A fragment of the submitted layout is presented in Fig. 3. In this circuits we intend to use biasing resistors on chip (shown in green). We have placed on chip three different types of control lines: (i) an antisymmetric line to change antisymmetric part of the flux through the qubit cells (in Fig. 3 it is situated to the right of the qubit), (ii) a symmetric line to control the working point  $r$  (to the left of the qubit in Fig. 3), and (iii) two lines for biasing the readout SQUID (below the qubit in Fig. 3).

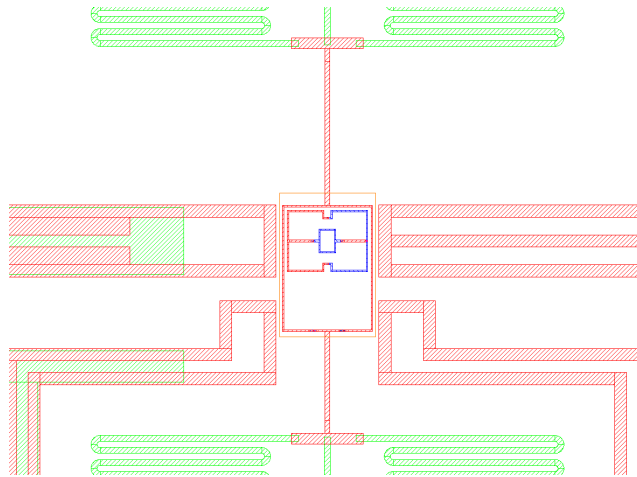


Figure 3: A part of the design submitted to the MIT Lincoln Laboratory.

In October 2007 we received two batches of Nb/ $\text{AlO}_x$ /Nb junction chips fabricated according to our design at MIT Lincoln Laboratory. Every chip contains three sets of structures designed for critical current densities of  $500 \text{ A/cm}^2$ ,  $1 \text{ kA/cm}^2$  and  $2 \text{ kA/cm}^2$ . Every set consists of three qubit circuits with different coupling strength between the readout SQUID and the qubit and four single Josephson junctions which have the same sizes as junctions in the qubit and the readout SQUID. We use them for testing purposes. In qubit circuits we use junctions of three different areas. To check the process reproducibility at a small scale, two test junctions have the size equal to the size of the smallest qubit junctions.

Figure 4 shows an SEM micrograph of a two-cell flux qubit together with its readout SQUID.

The fabrication process is characterized by a process bias, which determines a reduction of the electrical junction sizes from the drawn sizes. The average process bias in the batch delivered by Lincoln Laboratory is about  $0.25 \mu\text{m}$ . This value was taken into account when designing the qubits. Larger process biases result in increasing the maximal barrier height and decreasing of the qubit flux signal. Smaller process biases result in decreasing of the maximal barrier height, this makes qubit operating difficult. However, there is a variation across the wafer and from wafer to wafer. For the wafer DSM3\_07\_3.8 the process bias is  $0.23 \pm 0.03 \mu\text{m}$ . The dies with the process bias close to  $0.25 \mu\text{m}$  had smaller yield of junctions. The yield for those chips is seven working junctions out of eleven drawn, the median yield over

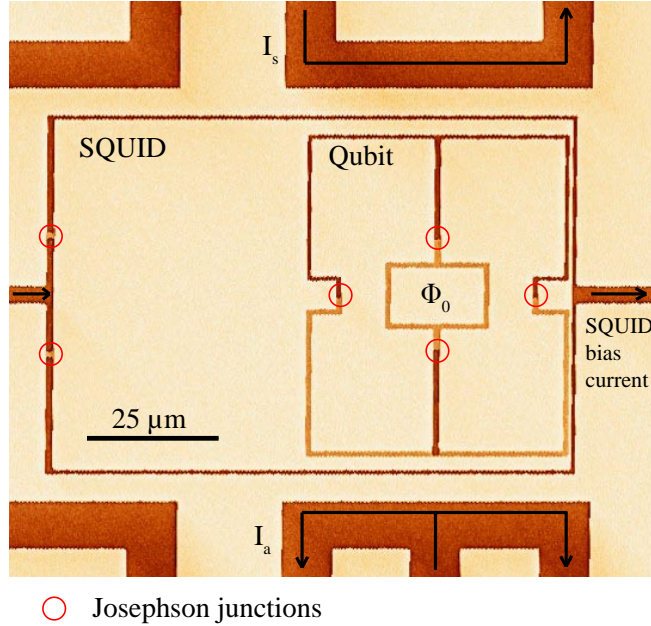


Figure 4: An SEM micrograph of a sample fabricated at MIT Lincoln Laboratory.

the wafer is nine working junctions. The yield estimate includes the drawn  $0.2 \mu\text{m}$  and  $0.3 \mu\text{m}$  Josephson junctions. The smallest junction reliably yielded has the drawn size of  $0.4 \mu\text{m}$ , while the smallest qubit junction has the drawn size of  $0.45 \mu\text{m}$ . For the wafer DSM4\_07\_11\_4 the process bias is  $0.21 \pm 0.04 \mu\text{m}$  and the median yield is eight working junctions out of nine drawn. The smallest junction has the drawn size of  $0.4 \mu\text{m}$ . The chip B4 is the only die with the process bias equal to  $0.25 \mu\text{m}$  on this wafer. There are several dies with process bias  $0.26 \mu\text{m}$  and  $0.27 \mu\text{m}$  on the wafer, but the expected qubit signals on these chips might be too weak, as the critical current density on these dies is around  $440 \text{ A/cm}^2$ . Thus only few chips from the available batch were expected to be close to the targeted parameters.

### 1.2.2 Measurements

The test Josephson junctions showed high-quality current-voltage characteristics, which are presented in Fig. 5. By scaling these curves we can calculate sizes of the junctions. The small qubit junctions have area of about  $0.03 \mu\text{m}^2$ , the large qubit junctions are of about  $0.08 \mu\text{m}^2$  and the large SQUID junctions have the area of about  $0.16 \mu\text{m}^2$ . These values are close to designed values, which were  $0.03 \mu\text{m}^2$ ,  $0.07 \mu\text{m}^2$  and  $0.14 \mu\text{m}^2$  respectively, and suitable for qubit operating. One can readily see that the spread in critical currents of two smallest qubit junctions is negligible.

Figure 6 shows measured current-voltage characteristics of readout SQUIDs on the chip C4 from the wafer DSM3\_07\_3\_8 and on the chip B4 from the wafer DSM4\_07\_11\_4. Despite the high quality of the test junctions, the critical current of the readout SQUID is much below the expected value. There is no peculiarity around  $3 \text{ mV}$ , which should correspond to  $2\Delta/e$ , where  $\Delta$  is the superconducting energy gap of niobium. We find a step around  $1 \text{ mV}$  for the wafer DSM3\_07\_3\_8 and  $0.4 \text{ mV}$  for the wafer DSM4\_07\_11\_4, which can most probably be due to difference of energy gaps in top and bottom niobium electrodes. We measured six chips from both wafers, and all 15 measured readout SQUIDs had the current-voltage characteristics similar to ones presented in Fig. 6. A couple of SQUIDs showed clear indications of shorts, but they might have been destroyed by an electro-static discharge during mounting procedure.

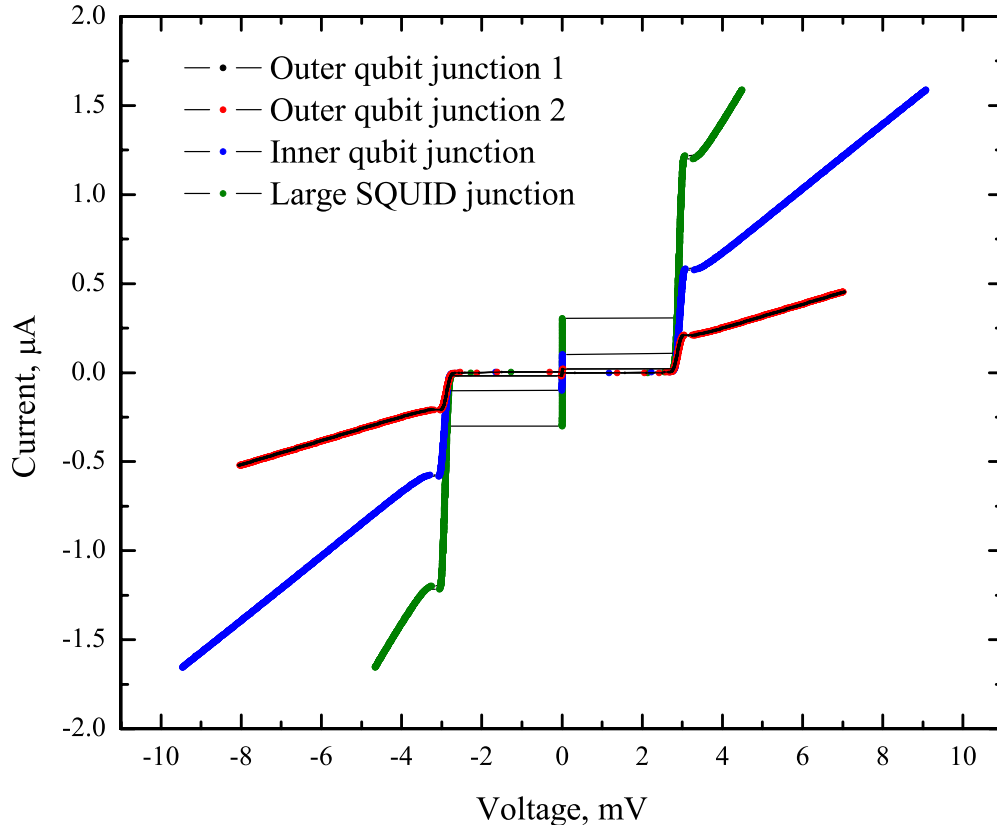


Figure 5: Current-voltage characteristics of the test junctions on chip C4 from the wafer DSM3.07\_3.8 at 300 mK.

We observed a modulation of the SQUID critical current with applied magnetic flux. The dependence of the SQUID critical current on symmetric control flux induced by control line  $I_s$  for the readout SQUID on the chip B4 from the wafer DSM4.07\_11.4 is presented in Fig. 7. The plot shows that the SQUID has non-zero sensitivity at zero external magnetic field. This allows us to read the qubit state out around zero symmetric control flux.

We believe that the zero-field response of the circuit is due to an odd number of flux quanta trapped in the passive  $\pi$ -shifter loop while cooling down. We made three attempts to trap flux inside the passive  $\pi$ -shifter loop. Making further tries turned impossible due to rapid degradation of the readout circuit. We saw a shift of the dependence of the SQUID critical current on the control current  $I_s$  after every attempt, which means that we trapped a different number of quanta. However, every time we trapped an odd number of quanta, as we saw the qubit switching at zero applied symmetric flux.

Figure 8 shows the dependence of the readout SQUID on chip B4 from the wafer DSM4.07\_11.4 critical current on antisymmetric control flux at zero applied symmetric flux. The dependence is non-monotonic around zero flux, which meets our expectation. At zero symmetric flux, we expect a switching of the qubit from one classical state to another, which changes the magnetic flux penetrating the readout SQUID loop. However, the measured curve does not look like an abrupt switching, as we see a slow change of the flux instead. We suppose that our antisymmetric control line current  $I_a$  changes both symmetric and antisymmetric flux, *i.e.* both the height of the potential barrier and the symmetry of the potential. This we are going to fix in the next run by changing the bonding scheme of the sample. Our current bonding scheme would work with equal contact resistances at the ground pads of the antisymmetric control line, which is a rather naive assumption. We believe that the differ-

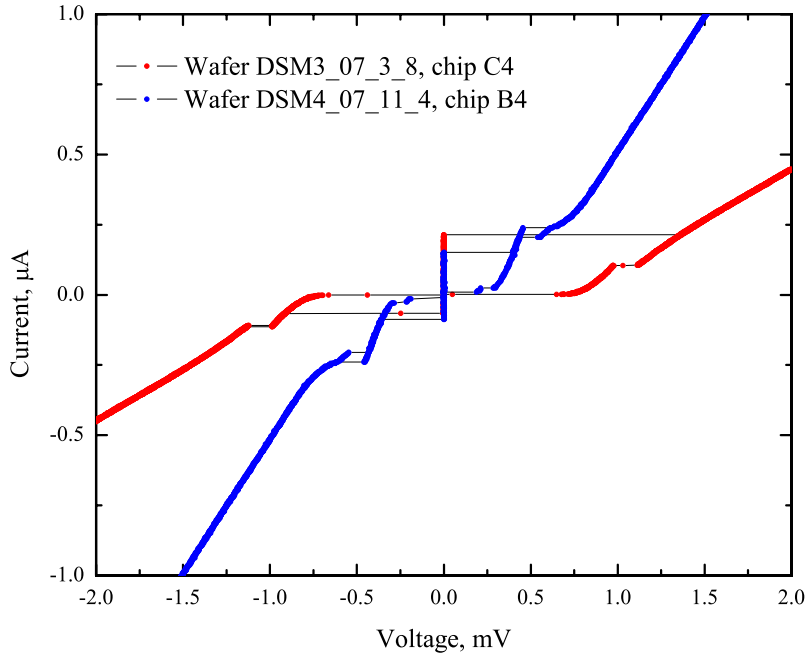


Figure 6: Current-voltage characteristics of the readout SQUIDs at 300 mK.

ence in contact resistances causes unequal current distribution between the branches of the antisymmetric control line. We are going to change the bonding scheme in order to have the only ground pad in the line, so that the distribution of the current in the line will not depend on contact resistances. Another possible reason for the smeared response is the temperature of this measurement of about 300 mK, which is rather high.

### 1.2.3 New design submitted to MIT Lincoln Lab

Upon consulting with Dr. William Oliver we have slightly changed sizes of Josephson Junctions in the readout DC SQUID to minimize the risk of damaging DC SQUID junctions during reactive ion etching fabrication steps. We also shunted DC SQUID junctions with capacitors to reduce quantum fluctuations and phase diffusion in the junctions, thus the shunting capacitors should increase resolution of our readout circuit. The new design was submitted to MIT Lincoln Laboratory in June 2008. We expect to receive new chips from MIT Lincoln Laboratory in November 2008.

## 1.3 Al/AlO<sub>x</sub>/Al junction based qubits

### 1.3.1 Fabrication in Erlangen

While waiting for chips ordered at MIT Lincoln Lab we tried to realize the design described above in Erlangen. Using on-chip biasing resistors required switching to a multilayer technological process. We also had to establish a process which would allow us to fabricate Josephson junctions of size down to  $0.1 \times 0.3 \mu\text{m}^2$ . It turned very difficult to fabricate such junctions reproducibly using our e-beam lithography system in Erlangen. For this reason, we obtained access to a high-end e-beam lithography system at the EU-funded facility in the department of Microtechnology and Nanoscience (MC2) at Chalmers University of Technology in Gothenburg, Sweden. This system based on JEOL JBX-9300FS e-beam machine is capable of writing a whole 3 inch wafer at once. Our approach was to make all the lithography steps using a full wafer at MC2, dice the wafer into chips  $5 \times 5 \text{ mm}^2$  in size, and finally fabricate

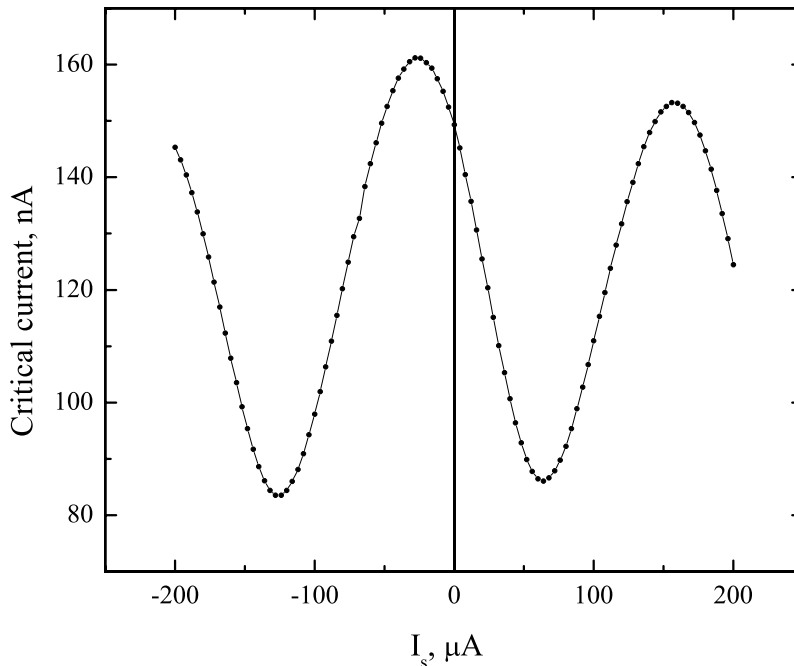


Figure 7: Dependence of the critical current of the readout SQUID on the chip B4 from the wafer DSM4.07.11.4 on symmetric control flux.

qubits together with readout circuits chip by chip by using our aluminum evaporation setup in Erlangen. In this procedure, we could still vary junction sizes and critical current density from chip to chip by controlling the evaporation angle and oxidation pressure and time.

To increase yield of working structures every chip designed for MC2 facility contained eight identical structures. One wafer contained 100 chips.

We divided the technological process into four steps:

1. making alignment marks;
2. depositing of palladium resistors;
3. definition of contact pads and control lines;
4. fabrication of qubits and readout circuits.

At every technological step we used lift-off process. E-beam lithography was performed at acceleration voltage of 100 kV in order to minimize the proximity effect. For the first three lithography steps, we used combinations of LOR A and UV5 resists because of a small exposure dose required for these combinations. Palladium resistors were deposited using electron beam evaporation technique at MC2. To achieve better adhesion, a thin layer of titanium was evaporated before palladium. Contact pads and control line were fabricated using thermal evaporation of aluminum at MC2. To have a better control of the undercut during the last lithography step we used high resolution electron beam resist ZEP 520A as top layer of the resist sandwich. The advantage of this resist is that its developer *o*-Xylene does not influence MMA-MAA resist that we used as bottom layer. Finally, we developed MMA-MAA resist in a mixture of isopropyl alcohol and deionised water. Unfortunately, during MMA-MAA resist prebaking there was an insulating polymer layer forming on top of the palladium layer. We have found that this layer can be destroyed by passing a dc current of about 0.5 mA through the contact pads. However, this procedure occasionally also destroyed Josephson junctions that we used in the readout circuit.

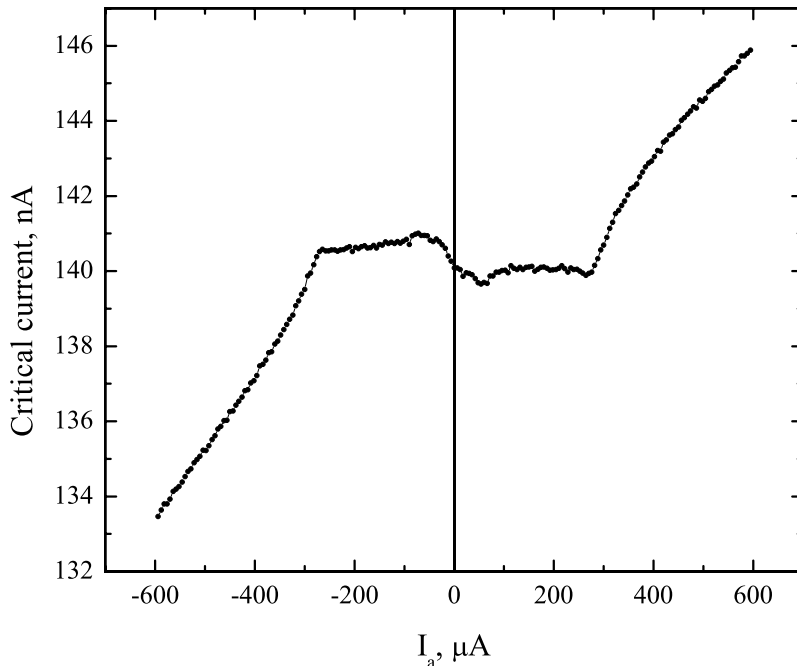


Figure 8: Dependence of the critical current of the readout SQUID on the chip B4 from the wafer DSM4.07.11.4 on antisymmetric control flux.

The SEM micrographs of the qubit and the readout circuit that we fabricated at MC2 and completed by aluminum evaporation in Erlangen are shown in Fig. 9. One can see that junctions have nearly rectangular shape. That makes evaluating of junctions areas easier and more precise, thus helping to calculate qubit parameters more accurately.

### 1.3.2 Measurements

We tested structures fabricated at MC2 at 300 mK. A current-voltage characteristic of a readout SQUID is presented in Fig. 10. One can readily see a step corresponding to four times the energy gap of aluminum that is a feature of three junction SQUID.

A dependence of the critical current of the readout SQUID on magnetic field is presented in Fig. 11. From this plot one can see that the SQUID has non-zero sensitivity at zero magnetic field, which in fact expected for the used three junction SQUID design.

We also tested the newly fabricated structures in our dilution refrigerator at about 25 mK. Unfortunately, we found that the electromagnetic noise was too high to get any reasonable results. Besides that, these structures turned out to be extremely sensitive to electro-static discharge (ESD) and several of them that we cooled down we destroyed. The most critical step for these samples was removal of polymer layer between palladium resistors and aluminum electrodes.

In order too minimize electromagnetic interference and noise, we have implemented a new wiring scheme in the dilution refrigerator. We deliver currents to the sample using single ended coaxial cables; the voltage drops will is measured using shielded twisted pairs. Current and voltage lines are spatially separated. This should reduce a crosstalk between voltage and current lines. We also use current dividers with ratio between 100 and 1000 as well as passive low-pass filters with cutoff frequency around 100 kHz.

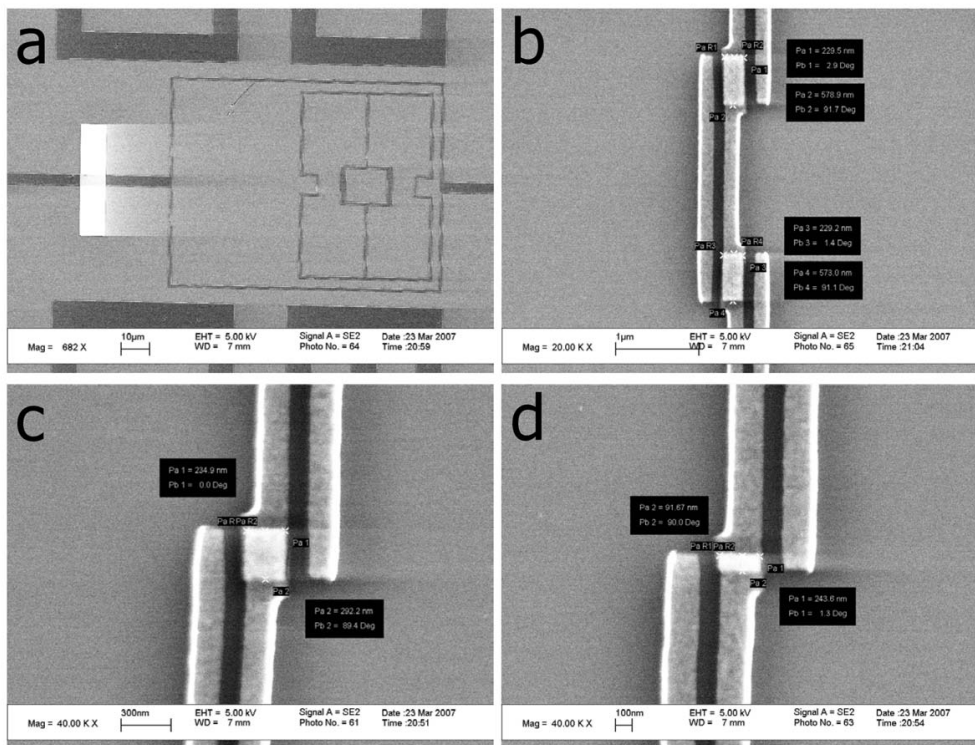


Figure 9: SEM images of a sample fabricated at MC2: a) the two-cell qubit with the readout SQUID; b) two larger junctions in the readout SQUID; c) inner qubit junction; d) outer qubit junction.

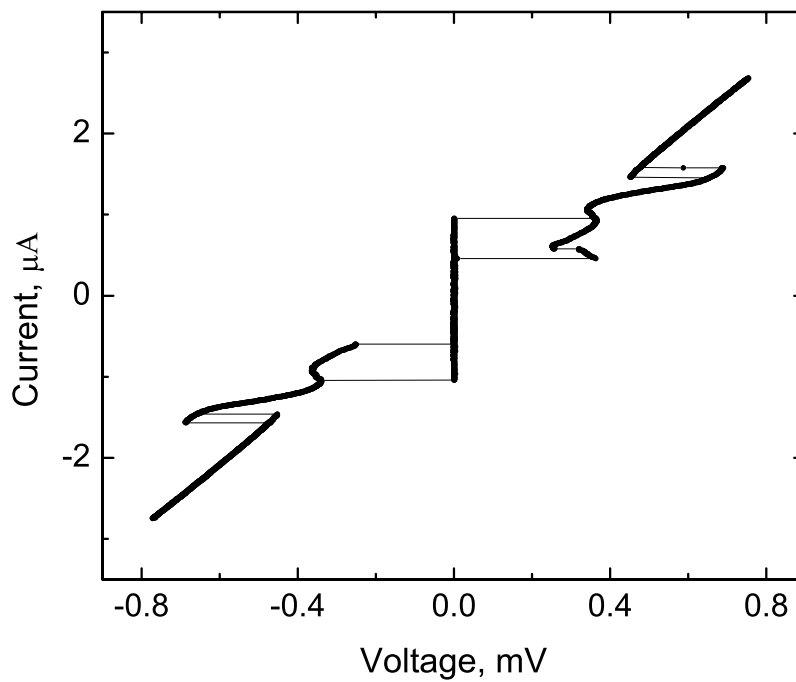


Figure 10: Current-voltage characteristic of the readout SQUID of MC2-made sample.

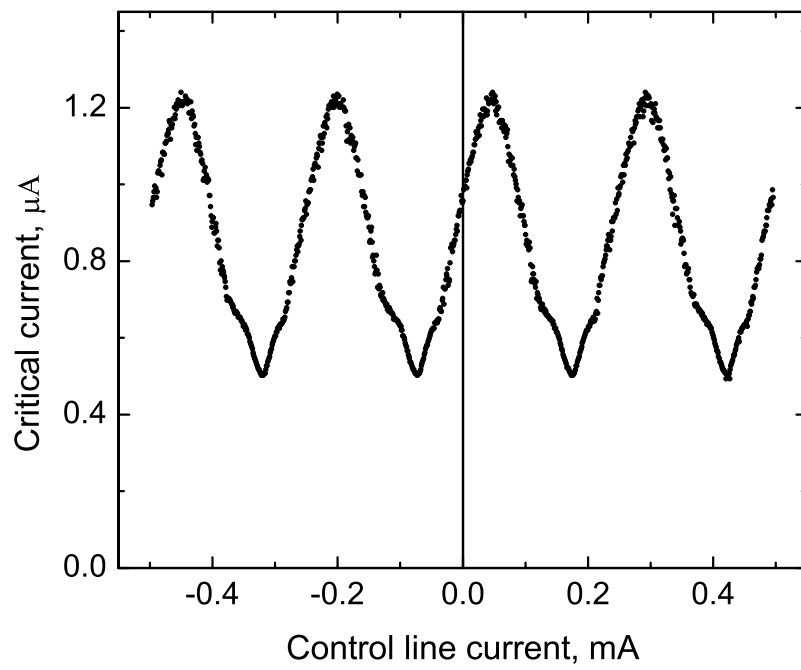


Figure 11: Dependence of the critical current of the readout SQUID of MC2-made sample on magnetic field.

## 2 High-contrast readout of superconducting qubits

### 2.1 Motivation

In the recent years, great progress has been achieved in experiments with superconducting circuits operated in the quantum coherent regime. At millikelvin temperatures, these circuits display quantized energy levels of which the lowest two are used to construct quantum bits [1, 2]. Among various qubit implementations, Josephson junction based qubits promise an outstanding scalability towards multi-qubit circuits and are conveniently controlled by dc and microwave frequency currents. The remaining major limitation of the superconducting approach to quantum computing is a relatively short coherence time of the qubit states.

An obvious source of decoherence for superconducting qubits is the coupling to a detector circuit necessary for the qubit readout. A strongly coupled detector maximizes readout contrast, while weaker coupling means a better isolation of the qubit thus facilitating longer coherence times. A weaker coupled detector disturbs the qubit less, traded for a loss of readout fidelity.

In this section, we describe the development of a data evaluation procedure which allows to maximize the qubit readout contrast also for a weakly coupled detector. We use this technique in experiments where we measure high-fidelity Rabi oscillations in Josephson phase qubits. To demonstrate its usefulness, we operate the phase qubit in an elevated temperature regime where the readout contrast is degraded by thermal fluctuations. We show that by using our new data evaluation method the full 100% readout contrast can be recovered.

### 2.2 The Josephson phase qubit

The logical states in experiments on Josephson phase qubits [3] and flux qubits [4] are distinguished by the magnetic flux which is generated by a persistent current in a superconducting loop. In all contemporary designs of these types of qubits, the qubit states are determined by a measurement of the switching current of a dc-SQUID used as a flux detector. The probabilities of the qubit states are thus obtained by a measurement of the statistical distribution of the SQUID switching current.

The Josephson phase qubit [3] consists of a superconducting loop interrupted by a Josephson junction. The complete qubit circuit includes a superconducting on-chip coil to provide for flux bias and an inductively coupled dc SQUID which is used as the detector for qubit readout. The phase difference  $\varphi$  of the superconducting order parameter across the junction depends on the magnetic flux threading the loop. The qubit loop inductance  $L$  is chosen such that the potential has the form of a double well. By changing the external magnetic flux, one potential well is made shallower while the other well becomes deeper.

The anharmonicity of the shallow well allows to construct a quantum bit by using the two levels of lowest energy as the logical states  $|0\rangle$  and  $|1\rangle$ . Initialization of the qubit is accomplished by setting the external magnetic flux to zero, where only one potential well exists, and then ramping up the flux adiabatically to the working point at which only a few energy levels remain in the well. Logical qubit operations are accomplished by resonant photon absorption of an applied microwave field which induces coherent (Rabi-) oscillation between the energy levels [3].

The phase eigenstates differ by the rate of quantum tunneling through the potential barrier which separates the shallow and deep wells. Measuring of the qubit is accomplished by a nanosecond-long pulse of magnetic flux which adiabatically reduces the depth of the shallow well. Its amplitude is adjusted such that tunneling to the deep well occurs only from the excited qubit state. The readout pulse therefore maps the logical qubit states  $|0\rangle$  and  $|1\rangle$  to the states  $|L\rangle$  and  $|R\rangle$  localized in separate potential wells. Since neighboring potential wells

correspond to states of opposite circulation direction of the loop current, a transition from the shallow to the deep well results in a change of magnetic flux [5].

### 2.3 Switching-current readout using a dc-SQUID

The magnetic flux in the qubit loop is detected using an inductively coupled dc-SQUID by determining its switching current from the superconducting to resistive state. The dc-SQUID switching current is measured by increasing its bias current until a voltage appears across the SQUID [6]. By repeating the qubit preparation and readout procedure several thousand times, a statistical switching current distribution is acquired. The mean switching current depends mostly on the SQUID critical current, which is a function periodic in  $\Phi_0$ . Its standard deviation  $\sigma$  originates in the probabilistic nature of the switching process, and is affected by quantum, thermal and bias current fluctuations [7].

Distinguishing the qubit states  $|L\rangle$  and  $|R\rangle$  by a *single shot* switching current measurement is only possible if the histograms corresponding to the two states do not overlap. This requires that the difference between the mean switching currents is about four times larger than the standard deviation. The change of the qubit persistent current  $\Delta I_p \approx I_c$  due to an inter-well transition generates a flux change  $\Delta\Phi_{\text{sq}} = M\Delta I_p$  in the readout SQUID. The resulting shift of the mean switching current depends on the dc-SQUID bias flux and its critical current modulation depth. The latter is reduced [8] to below 50 % if the dc-SQUID inductance  $L_{\text{sq}}$  and critical current  $I_{c,\text{sq}}$  are large so that  $L_{\text{sq}}I_{c,\text{sq}}/\Phi_0 > 1$ .

To reach the single shot readout limit, a typical minimal flux signal from the qubit should be about  $10\text{ m}\Phi_0$ , requiring a mutual inductance of  $M \approx 20\text{ pH}$  at a qubit junction critical current of  $I_c = 1\mu\text{A}$ . The mutual inductance mediates dissipation in the dc-SQUID and generates back-action to the qubit. While the back-action scales as  $M^2/LL_{\text{sq}}$ , dissipation induced in the qubit is proportional to the inverse effective dc-SQUID damping impedance  $Z_{\text{sq}}^{-1}$ , which is transformed to the qubit via  $Z^{-1} = Z_{\text{sq}}^{-1}(M/L)^2$ . A quadratic benefit is hence expected from a reduced mutual inductance.

In practical qubit measurements, statistics about the state population are always acquired because of the probabilistic nature of quantum mechanics. A single shot measurement is therefore not mandatory as long as it remains possible to reconstruct the individual qubit state contributions from the statistical data set with high enough fidelity.

### 2.4 Data evaluation procedure

Our new method of reconstructing the qubit state population from overlapping SQUID switching current histograms is the following. The qubit is first prepared in state  $|L\rangle$  and the switching current probability histogram  $P(I)$  generated by this state is recorded. This histogram is fitted to an arbitrary function  $f_L(I)$ . For simplicity, we are using a 10 degree polynomial truncated between minimal and maximal measured switching currents as the fitting function  $f_L(I)$ . An alternative fitting to a physically correct distribution, which is an integral function of the exponential escape rate, is also possible but requires more computing time and an adaption of the model depending on the sample. The same procedure is repeated for a histogram obtained from measurements of a qubit prepared purely in the state  $|R\rangle$ , thus obtaining the fitting function  $f_R(I)$ . All further overlapping histograms are then fitted to the function

$$P(I) = P(|1\rangle) f_R(I) + [1 - P(|1\rangle)] f_L(I), \quad (3)$$

hereby obtaining  $P(|1\rangle)$ , the population of the excited qubit state  $|1\rangle$ , as the only fitting parameter.

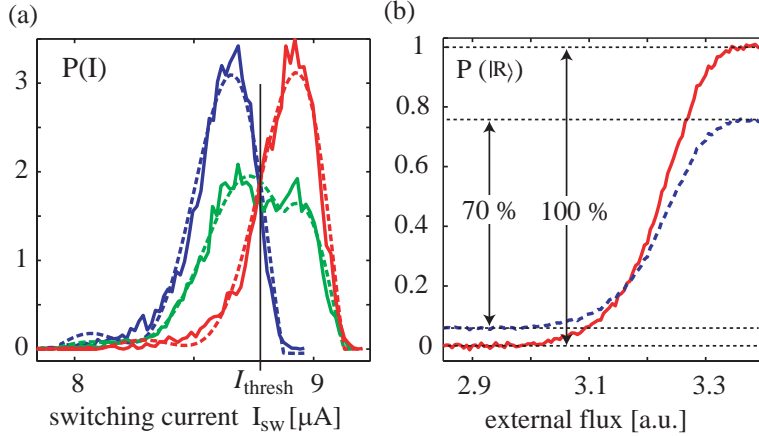


Figure 12: (a) Switching current distributions of a dc-SQUID broadened by thermal fluctuations at  $T = 275$  mK. Left and right histograms correspond to the qubit being in state  $|L\rangle$  and  $|R\rangle$ , respectively. The intermediate histogram corresponds to equal probability of the two states. Dashed lines are polynomial fits. (b) The probability to measure the state  $|R\rangle$  versus externally applied flux. The dotted curve is calculated using the standard method, resulting in a maximum contrast of 70%. The solid curve has been obtained from weighted fits to the histograms, which reconstruct the two states with 100% contrast.

## 2.5 Experimental results

Figure 12(a) shows histograms of the phase qubit prepared in states  $|L\rangle$ ,  $|R\rangle$  and in a superposition state together with the fitting functions  $f_L(I)$  and  $f_R(I)$  drawn as dashed lines. The standard single shot method of obtaining the qubit population is by setting a threshold value  $I_{\text{thresh}}$  of switching current and counting the number of counts above this threshold  $N(I_{\text{sw}} > I_{\text{thresh}})$  relative to the total number of events  $N$ ,

$$P(|1\rangle) = \frac{N(I_{\text{sw}} > I_{\text{thresh}})}{N}. \quad (4)$$

A loss of readout contrast here occurs because of switching current events lying in the region of overlapping histograms, which can not be attributed to one or other state. This reduced contrast is shown in Fig. 12(b) by the dashed curve calculated according to Eq. (4). The alternative procedure of extracting the excited qubit state population  $P(|1\rangle)$  by using Eq. (3) is shown in Fig. 12(b) by solid line. One can see that it restores the full 100% contrast.

To illustrate the benefit of our readout contrast enhancement procedure, in Fig. 16 we show a Rabi oscillation measurement with a phase qubit [9], provided to us by the UCSB group. Here we evaluate the data with both the standard threshold and histogram fitting methods. While at the lower temperature the histograms are narrow enough to nearly reach the single shot readout, at the higher temperature thermally broadened histograms are overlapping. The reduction of the Rabi oscillation amplitude due to this overlap is fully eliminated by using the fitting procedure.

## 2.6 Application in multi-qubit circuits

The technique demonstrated above appears promising for reading out multi-qubit circuits. The number of necessary readout SQUIDs can be reduced by weakly coupling several qubits to a single dc-SQUID and employing the fitting procedure to reconstruct the individual qubit flux states. After completion of a quantum algorithm, each qubit generates a flux signal in

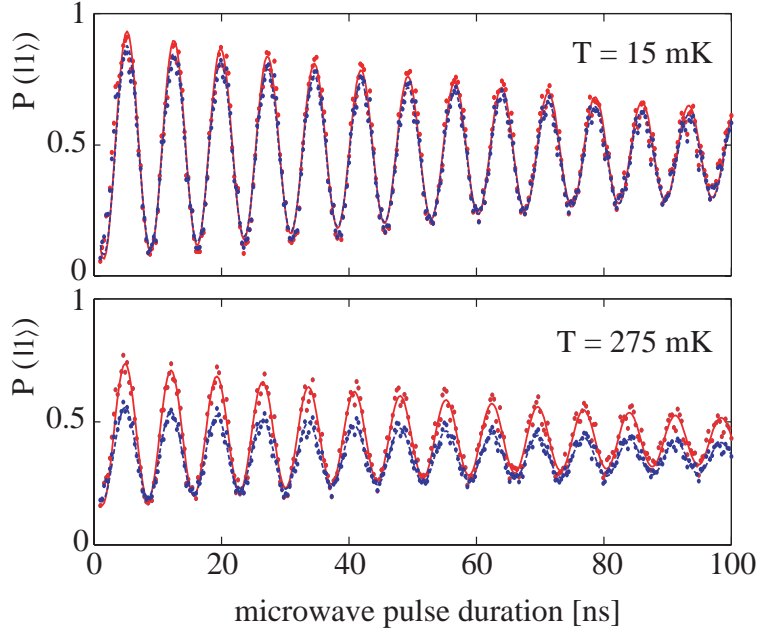


Figure 13: Rabi oscillation in the excited qubit state, measured at temperatures of 15 mK (top) and 275 mK (bottom). Blue data points (fitted by dashed line) are obtained by the standard evaluation method. A loss of oscillation visibility due to thermal histogram broadening is avoided by the weighted fit evaluation, resulting in the red data points (solid line).

the dc-SQUID of

$$\Delta\Phi_{\text{sq}} = \sum_i M_i \Delta I_{c,i}, \quad (5)$$

where  $\Delta I_{c,i}$  is the signal from qubit  $i$  and  $M_i$  is the mutual inductance between qubit  $i$  and the dc-SQUID. Our estimate shows that for two qubits the ratio  $M_2/M_1$  must be a factor of two to be able to distinguish the four possible states. Our method allows to reduce the coupling strength to the dc-SQUID for all qubits, thus avoiding decoherence.

### 3 Josephson phase qubits

A vital factor in research progress on macroscopic quantum coherent circuits is to obtain an understanding of the nature and origin of decoherence. Obvious sources of decoherence that affect superconducting qubits are bias current and magnetic field fluctuations, which can be controlled by a proper experimental setup. Recently, the importance of the material properties of the Josephson junction barrier was realized by the UCSB group led by John Martinis, resulting in an immediate prolongation of the coherence time by a factor of about 20. However, until now this group did no systematic experimental study of the influence of temperature on superconducting qubits. Common notion shared by the superconducting qubit community is that good qubit performance can only be obtained at temperatures below 100 mK, whose generation requires expensive and bulky dilution refrigerators.

In contrast to the above mentioned common believe, our latest experimental results reported below show that operation of Josephson phase qubits is possible at temperatures much higher than 100 mK. We found that the highest temperature where coherent Rabi and Ramsey oscillation can be observed is limited by the qubit energy level splitting which is determined by the circuit design. Beneath providing additional hints towards a better understanding of decoherence in superconducting circuits, these new findings have appealing implications

concerning the realization of solid-state quantum computing. Commercially available cryogen-free He<sup>3</sup> cryostats appear to be sufficient to cool the qubit chip, simplifying both research and operation of quantum computers.

As the logical qubit states  $|0\rangle$  and  $|1\rangle$ , a phase qubit uses the lowest two energy eigenstates of the Josephson phase in a metastable potential well of a current-biased junction. An elegant way to decouple the junction from the electromagnetic environment is by applying its bias current through a dc-transformer [5], hereby embedding the junction in a superconducting loop as it is shown in Fig. 14(a). The resulting circuit is known as an rf-SQUID and has a potential energy

$$U(\varphi) = \frac{\hbar I_C}{2e} \left( 1 - \cos \varphi + \frac{1}{2\beta_L} \left( \varphi - 2\pi \frac{\Phi_{\text{ext}}}{\Phi_0} \right)^2 \right), \quad (6)$$

where  $\varphi$  is the phase difference across the junction,  $I_C$  is its critical current,  $\Phi_{\text{ext}}$  the externally applied flux through the qubit loop, and  $\Phi_0$  is the superconducting flux quantum. The qubit loop inductance  $L$  is chosen such that the parameter  $\beta_L = 2\pi L I_C / \Phi_0 \approx 4$ , resulting in a double well potential plotted in Fig. 14(b). By changing the flux  $\Phi_{\text{ext}}$ , one of the wells can be made shallow enough such that it contains only a small number of energy levels. The excited state  $|1\rangle$  is populated by resonant photon absorption of an applied microwave field which induces coherent Rabi oscillation between the energy levels. Reading out the state population is done by using a nanosecond long but still adiabatic dc-pulse of magnetic flux, which reduces the height of the barrier separating the wells. The pulse amplitude is adjusted such that an inter-well transition occurs only from the excited state. Since each potential minimum corresponds to a certain circulation direction of the loop current, the transition from the shallow to the deep well results in a change of magnetic flux, which is afterwards read out by recording the switching-current distribution of an inductively coupled dc-SQUID.

### 3.1 Samples

We studied the influence of temperature on qubit performance using two different samples. Sample #1 was fabricated according to our designs at VTT foundry [10] using a standard lithographic Nb/AlO<sub>x</sub>/Nb-trilayer processes, featuring Josephson junctions of 7 μm<sup>2</sup> minimum area and 30 A/cm<sup>2</sup> current density. Sample # 2 has been fabricated by John Martinis group at UCSB in a custom process, using aluminum as the electrode material and a small qubit junction of size approximately 1 μm<sup>2</sup>. In contrast to the standard VTT samples featuring SiO<sub>2</sub> insulation, in the UCSB sample SiN<sub>x</sub> is used as the dielectric.

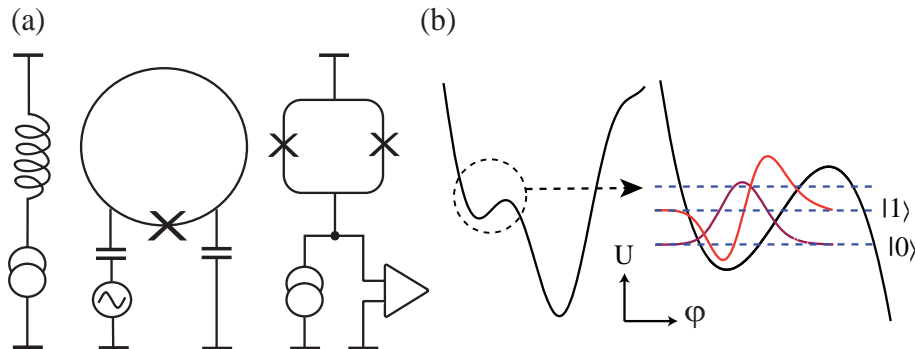


Figure 14: (a) Schematic of the phase qubit circuit. The qubit junction is embedded in a superconducting loop which is coupled inductively to the flux-biasing coil and readout dc-SQUID. (b) Sketch of the qubit potential  $U(\varphi)$ . On the right side, a zoom into the shallow left potential well indicates the wave functions describing the two qubit states  $|0\rangle$  and  $|1\rangle$ .

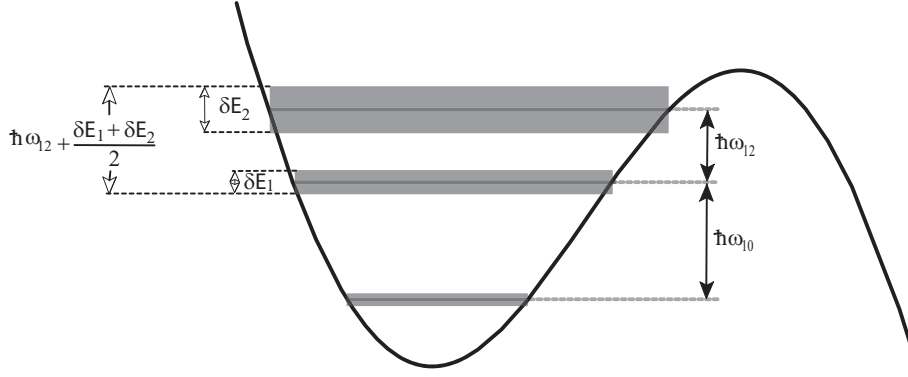


Figure 15: The widths  $\delta E_n$  of the energy levels  $n$  are indicated by grey bars and the energy level separations are shown by black arrows.

The UCSB group has demonstrated recently [11] that minimizing the junction area and thus the number of two-level fluctuators in the junction tunnel barrier significantly improves qubit performance. Tuning the junction capacitance in the appropriate range is achieved by using a silicon nitride capacitive element separated on chip from the Josephson tunnel junction.  $\text{SiN}_x$  does not suffer from two-level fluctuators and thus has much lower dielectric loss compared to the oxide dielectrics  $\text{SiO}_2$ . Accordingly, measurements of the UCSB sample #2 in our setup showed coherence times which were by more than one order of magnitude longer than in the Nb  $\text{SiO}_x$  based sample #1.

### 3.2 Spectroscopic quality factor

To measure the life time  $T_1$  of the excited state we apply a resonant microwave  $\pi$ -pulse which prepares the qubit in the excited state. Then, after a variable delay time, we measure the remaining population in the excited state. We observed exponential decay at half-life times of about 4 ns for sample #1 and about 90 ns for sample #2.

Quantum mechanically, the life time  $T_1$  is related to an uncertainty in the energy of the excited state, giving rise to a broadening  $\delta E$  of the level at energy  $E$  as it is sketched in Fig. 15. Therefore, in consistence with the measured  $T_1$  relaxation times, we observed that the spectroscopic resonance peak for photon activation to the excited state has a width in frequency  $\delta\omega$  of about  $2\pi \cdot 10$  MHz for sample #2 and about  $2\pi \cdot 400$  MHz for sample #1. Corresponding  $Q$  factors calculated by

$$Q = \frac{\omega}{\delta\omega} = \frac{E}{\delta E} \quad (7)$$

were about 30 at a transition frequency  $\omega_{01} = 2\pi \cdot 16.5$  GHz for the sample #1 and about 600 at a frequency  $\omega_{01} = 2\pi \cdot 8$  GHz for sample #2. The anharmonicity of the qubit potential has the consequence that the separation between adjacent levels decreases with increasing energy. An external microwave will hence be resonant only to one transition, provided that the individual levels are not too broad. From Fig. 15 it can be seen that this corresponds to the condition

$$\hbar\omega_{12} + \frac{1}{2}(\delta E_1 + \delta E_2) \ll \hbar\omega_{01}, \quad (8)$$

where  $\delta E_n$  is the full width of level  $n$  arising from its finite lifetime  $\Gamma_n^{-1}$  and  $\omega_{mn}$  is the transition frequency from level  $m$  to level  $n$ .

It is important to note that the qubit potential well, as its depth is increased, becomes more harmonic and the difference in the transition frequencies between neighboring levels

gets smaller. Taking into account the broad resonance line width of Nb-based qubit #1, we can therefore not regard this qubit as a two-level system, but should rather expect multilevel dynamics [12]. In contrast, sample #2 is operated by applying microwaves as a true two-level system due to its high  $Q$  value. Deeper potential well thus remains anharmonic enough not to result in populating of higher energy levels by microwave applied at  $\omega_{01}$ .

### 3.3 Coherent oscillation at high temperatures

We observed Rabi oscillation in the population of the excited state by varying the duration of a microwave pulse which frequency is resonant to the  $|0\rangle$  to  $|1\rangle$  transition. By fitting the data to an exponentially damped sine function, we extract Rabi amplitude, frequency and decay time. The above reported Nb-based phase qubits show rather modest decoherence times, where samples from VTT perform very similarly to our previously measured Hypres samples. In these Nb-based qubits  $T_1$  as well as Rabi decay time  $T_R$  were typically 3 to 7 ns, which is significantly shorter than the data for Al-based circuits.

In order to observe Rabi oscillation at higher temperatures, we have to avoid thermal activation out of the shallow potential well. The activation rate increases as the potential barrier height becomes comparable to the thermal energy  $k_B T$ . By reducing the field bias and operating in a deeper potential well, we were able to observe oscillations at temperatures up to 0.9 K in the Nb-based qubit #1. At a temperature of 0.8 K, the amplitude was reduced by a factor of one half, while the oscillation decay time dropped only by 80%, see Fig. 17.

We found that, above a certain temperature, it becomes necessary to reduce the amplitude of the readout pulse in order to preserve good contrast of oscillations. This is due to the fact that, during the readout pulse, activation from the excited qubit state to the deep well becomes possible not only by quantum tunnelling but also by thermal activation over the barrier. Moreover, at higher temperatures the width of the measured switching-current histogram of the readout dc-SQUID increases. We were able to avoid a loss of contrast between the two qubit states due to broadened histograms by a fitting procedure extracting the additive weighted contributions of the two states.

Our results for the high- $Q$  sample #2 are summarized in Fig. 18. We plotted here the observed dependence of the Rabi oscillation amplitude and decay on temperature. Remarkably, we notice only a very small decrease of decoherence times at low temperatures. The oscillations disappear completely close to the temperature  $T = \hbar\omega/k_B$ , which is 355 mK at  $\omega = 2\pi \cdot 7.4$  GHz and 384 mK at  $\omega = 2\pi \cdot 8$  GHz.

To measure the influence of temperature on the dephasing time, in sample #2 we performed a Ramsey-type experiment, in which two  $\pi/2$ -pulses separated by a variable duration are applied to the qubit. As expected, the frequency of the observed Ramsey fringes was equal to the detuning of the microwave pulses. We took a set of data at 335 MHz below the exact resonance at 8 GHz. Figure 19 shows the Ramsey oscillation amplitude and extracted  $T_2$  time versus temperature. These oscillations decay similarly to the Rabi data.

## 4 Summary and conclusion

We redesigned our structures to realize the newly proposed “silent” two-cell qubits. At the operating point, the “silent” qubit should be insensitive to fluctuations caused by the flux control circuits. We optimized our design for different critical current densities and submitted it to MIT Lincoln Laboratory. We have observed a switching of the two-cell flux qubit with a passive  $\pi$ -shifter between two classical states during a characterisation experiment of chips fabricated at MIT Lincoln Laboratory. The qubit switches around zero

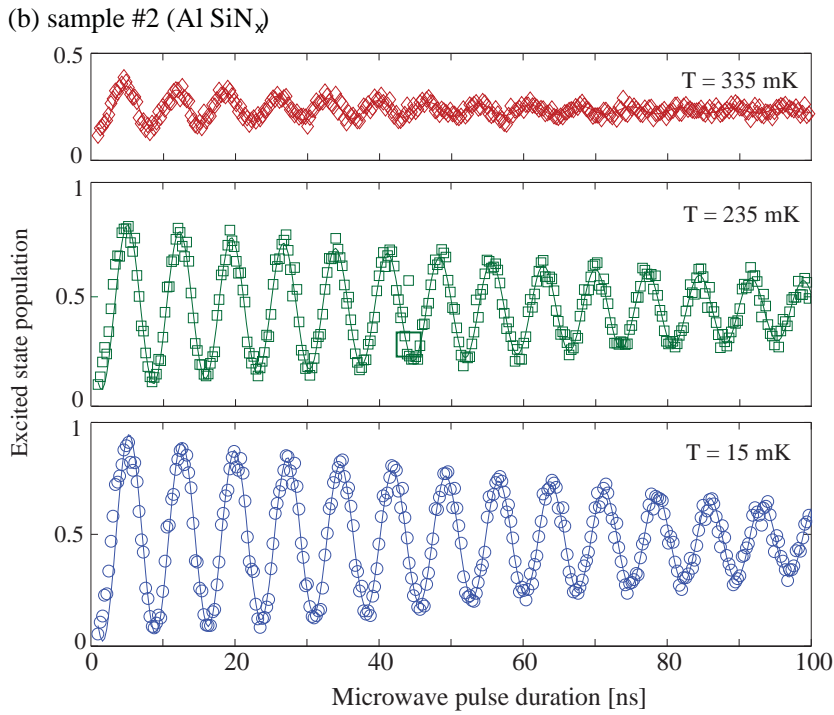
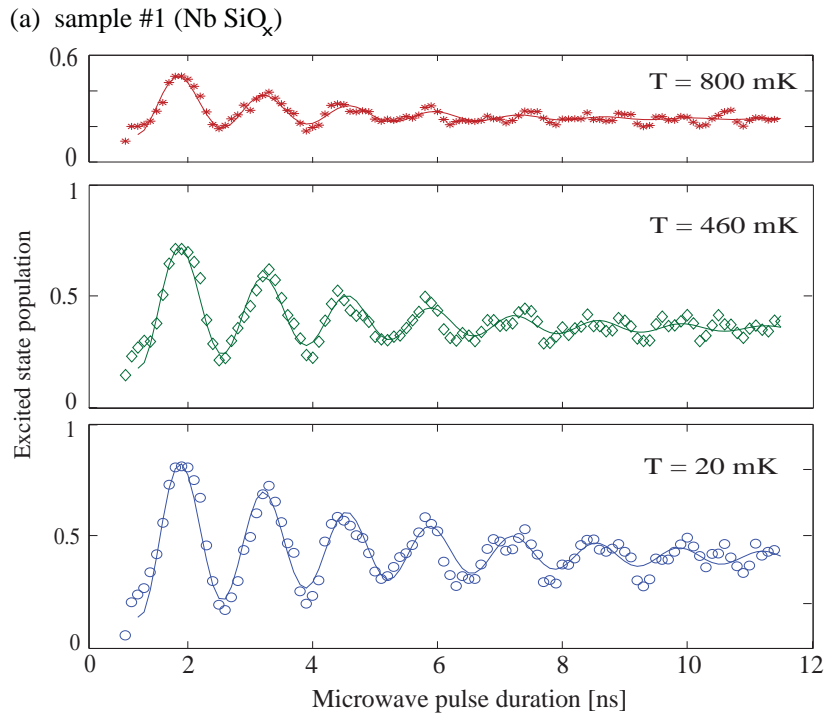


Figure 16: Rabi oscillations observed in Nb-SiO<sub>x</sub> based qubit sample #1 (a) and Al-SiN<sub>x</sub> based qubit sample #2 (b), at the indicated temperatures. Solid lines are a fits to an exponential decaying sine functions from which Rabi amplitude and decay time are extracted.

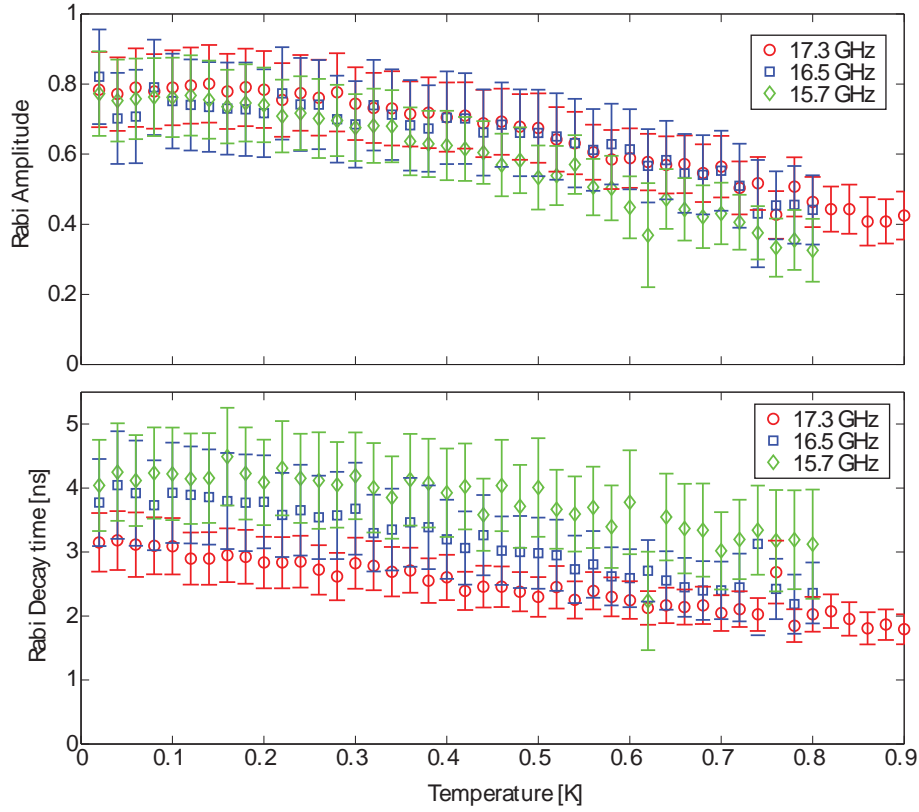


Figure 17: Rabi oscillation amplitude (top) and decay time (bottom) versus temperature, measured using sample #1. Each data set correspond to an adjusted magnetic field resulting in resonance at the frequency indicated in the legend.

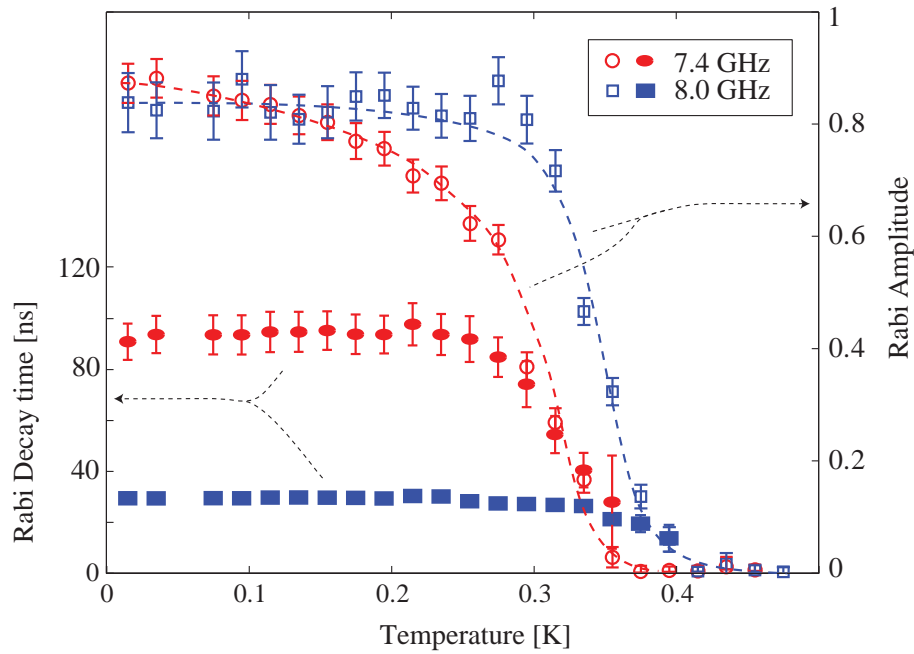


Figure 18: Amplitude (right axis) and decay time (left axis) of Rabi oscillation observed in sample #2, plotted versus temperature. Each set of data points corresponds to an adjusted magnetic field bias resulting in an energy level spacing causing resonance at the microwave frequency indicated in the legend. Dashed lines are guides to the eye.

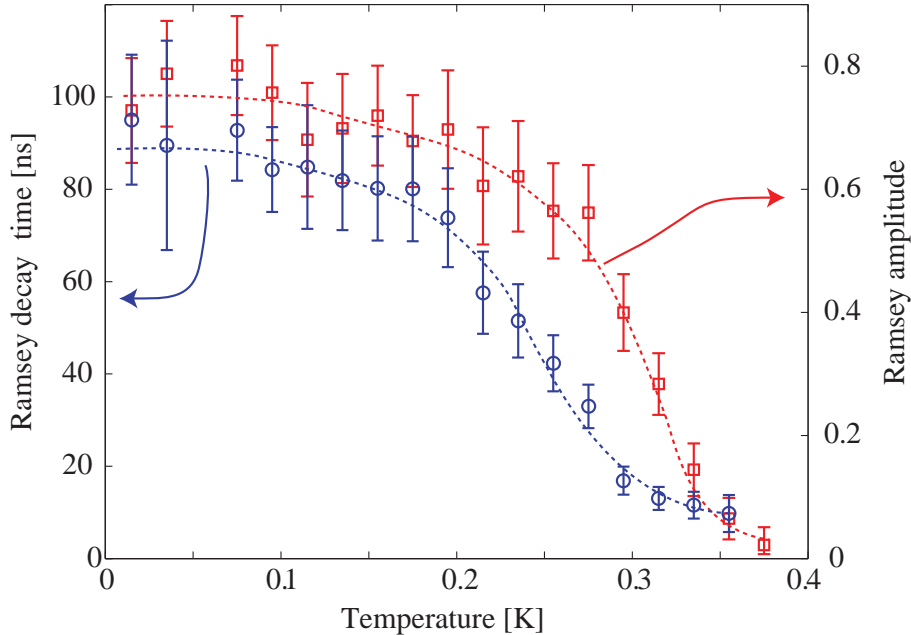


Figure 19: Ramsey oscillation amplitude (right axis) and decay time (left axis) vs. temperature (sample # 2). Dashed lines are guides to the eye.

flux for both symmetric and antisymmetric flux components, which meets the expectation of our experiment. This behaviour minimises the coupling of the qubit to the environment.

We developed a new multilayer technological process consisting of fabrication of the structures partially at MC2 foundry at Chalmers University and finishing the fabrication in Erlangen. Using this process, we fabricated aluminum junctions as small as  $0.09 \times 0.24 \mu\text{m}^2$ , which meets the goal set for our experiment. We have revised noise issues and wiring in our dilution refrigerator. These measures helped us to reduce interference and channels cross-talk during measurements.

In the second part of the report we presented a new method of qubit data evaluation which makes it possible to enhance the readout contrast in experiments with superconducting qubits. This technique employs a weighted fitting of switching-current histograms obtained from the dc-SQUID detector, which is used for qubit readout. We demonstrated reconstructing of the full contrast of Rabi oscillation using a phase qubit in a regime where the oscillation visibility was reduced due to thermal fluctuations in the environment. Similarly, a large readout contrast can be obtained in qubit circuit designs where the detector SQUID is weakly coupled to the qubit. This feature is of particular importance, because for achieving long coherence times the qubits should be well isolated from the environment.

The demonstrated data evaluation procedure will be beneficial for multi-qubit circuits, offering an opportunity to read out the states of several qubits by a single dc-SQUID. We expect that it will be thus possible to reconstruct the individual qubit states with good fidelity.

In the last part of the report we presented Rabi oscillations in Josephson phase qubits fabricated using standard Nb process with  $\text{SiO}_x$  on-chip dielectric. Operating in a deep potential well, Rabi like oscillation persisted at temperatures up to 0.9 K, where only modest decrease in decay time was observed. These results are obtained in the multi-level limit. In contrast, Al based phase qubit with  $\text{SiN}_x$  dielectric in the shunting capacitor which we obtained from UCSB has long coherence times and can be treated as a true two-level system. Decoherence times measured in the UCSB sample are nearly independent of temperature up to the point at which the thermal energy becomes comparable to the energy level separation.

These results suggest that presently existing best phase qubits designed to have a high  $Q$  and large energy level separation could be easily operated at higher temperatures.

## References

- [1] J. Q. You and F. Nori, *Phys. Today* **58**(11), 42 (2005).
- [2] G. Wendin and V. Shumeiko, in *Handbook of Theoretical and Computational Nanotechnology*, edited by M. Rieth and W. Schommers (ASP, Los Angeles, 2006).
- [3] J. M. Martinis, S. Nam, J. Aumentado, and C. Urbina, *Phys. Rev. Lett.* **89**, 117901 (2002).
- [4] I. Chiorescu, Y. Nakamura, C. J. P. M. Harmans, and J. E. Mooij, *Science* **299**, 1869 (2003).
- [5] R. W. Simmonds, K. M. Lang, D. A. Hite, D. P. Pappas, and J.M. Martinis, *Phys. Rev. Lett.* **93**, 077003 (2004).
- [6] T. A. Fulton and L. N. Dunkleberger, *Phys. Rev. B* **9**, 4760 (1974).
- [7] A. Wallraff, A. Lukashenko, C. Coqui, A. Kemp, T. Duty and A. V. Ustinov, *Rev. Sci. Inst.* **74**, 3740 (2003).
- [8] B. Chesca, R. Kleiner and D. Koelle in *The SQUID Handbook, Vol. I: Fundamentals and technology of SQUIDS and SQUID systems*. Eds. J. Clarke and A. I. Braginski, Wiley-VCH, Weinheim, (2004) p. 43.
- [9] J. Lisenfeld, A. Lukashenko, M. Ansmann, J. M. Martinis, and A. V. Ustinov, *Phys. Rev. Lett.* **99**, 170504 (2007).
- [10] VTT Technical Research Center of Finland.
- [11] M. Steffen, M. Ansmann, R. McDermott, N. Katz, R. C. Bialczak, E. Lucero, M. Neeley, E. M. Weig, A. N. Cleland, and J. M. Martinis, *Phys. Rev. Lett.* **97**, 050502 (2006).
- [12] J. Claudon, F. Balestro, F. W. J. Hekking, and O. Buisson, *Phys. Rev. Lett.* **93**, 187003 (2004).